

**MODELING VENTRICULAR INTERACTION:  
A MULTISCALE APPROACH FROM SARCOMERE  
MECHANICS TO CARDIOVASCULAR SYSTEM  
HEMODYNAMICS**

JOOST LUMENS<sup>1,2</sup>, TAMMO DELHAAS<sup>1</sup>, BORUT KIRN<sup>2</sup>, THEO ARTS<sup>2</sup>

*Departments of <sup>1</sup>Physiology and <sup>2</sup>Biophysics, Maastricht University,  
Universiteitssingel 50, Maastricht, P.O. Box 616, The Netherlands*

*E-mail: j.lumens@fys.unimaas.nl; t.delhaas@fys.unimaas.nl;  
b.kirn@bf.unimaas.nl; t.arts@bf.unimaas.nl*

Direct ventricular interaction via the interventricular septum plays an important role in ventricular hemodynamics and mechanics. A large amount of experimental data demonstrates that left and right ventricular pump mechanics influence each other and that septal geometry and motion depend on transmural pressure. We present a lumped model of ventricular mechanics consisting of three wall segments that are coupled on the basis of balance laws stating mechanical equilibrium at the intersection of the three walls. The input consists of left and right ventricular volumes and an estimate of septal wall geometry. Wall segment geometry is expressed as area and curvature and is related to sarcomere extension. With constitutive equations of the sarcomere, myofiber stress is calculated. The force exerted by each wall segment on the intersection, as a result of wall tension, is derived from myofiber stress. Finally, septal geometry and ventricular pressures are solved by achieving balance of forces. We implemented this ventricular module in a lumped model of the closed-loop cardiovascular system (CircAdapt model). The resulting multiscale model enables dynamic simulation of myofiber mechanics, ventricular cavity mechanics, and cardiovascular system hemodynamics. The model was tested by performing simulations with synchronous and asynchronous mechanical activation of the wall segments. The simulated results of ventricular mechanics and hemodynamics were compared with experimental data obtained before and after acute induction of left bundle branch block (LBBB) in dogs. The changes in simulated ventricular mechanics and septal motion as a result of the introduction of mechanical asynchrony were very similar to those measured in the animal experiments. In conclusion, the module presented describes ventricular mechanics including direct ventricular interaction realistically and thereby extends the physiological application range of the CircAdapt model.

## **1. Introduction**

The left (LV) and right ventricle (RV) of the heart are pumping blood in the systemic and pulmonary circulation, respectively. Although both ventricular cavities are completely separated, there is a strong mechanical interaction between the ventricles, because they share the same septal wall, separating the

cavities. A vast amount of evidence demonstrates that septal shape and motion depend on transseptal pressure [1, 2]. Also, a change in pressure or volume load of one ventricle influences pumping characteristics of the other ventricle [3-5].

Various mathematical models have been designed to describe the consequences of mechanical left-right coupling by the septum for ventricular geometry and hemodynamics [6-11]. Commonly, interaction is assumed to be global and linear, using coupling coefficients for pressures, volumes or compliances. An exception was found in the model by Beyar *et al.* [6], which was based on the balance of forces between free walls and septum. The latter model was primarily designed for diastolic interaction and was not suited to implement the dynamic mechanics of myocardial contraction.

The CircAdapt model [12] has been developed to simulate cardiovascular dynamics and hemodynamics of the closed-loop circulation. The model is configured as a network, composed of four types of modules, i.e., cardiac chamber, blood vessel, valve and flow resistance. The number of required independent input parameters was reduced tremendously by incorporating adaptation of geometry, e.g., size of ventricular cavities and thickness of walls, to mechanical load so that stresses and strains in the walls were normalized to physiological standard levels. Ventricular interaction was modeled as an outer myocardial wall, encapsulating both ventricles, and an inner wall around the LV cavity accommodating the pressure difference between LV and RV. This description is reasonable, as long as LV pressure largely exceeds RV pressure. However, for high RV pressures, the description is not accurate anymore.

Because of the need to describe pathologic circumstances with high RV pressure, a new model of left to right ventricular interaction was designed. This model should be symmetric in design, allowing RV pressure to exceed LV pressure. Furthermore, the new model should satisfy the following requirements to fit in the CircAdapt framework. 1) For given LV and RV volumes as input, LV and RV pressures should be calculated as a result. 2) The model should incorporate dynamic myofiber mechanics, responsible for pump action. 3) The model should satisfy conservation of energy, i.e., the total amount of contractile work, as generated by the myofibers, should equal the total amount of hydraulic pump work, as delivered by the ventricles.

In the present study, a model setup was found, satisfying abovementioned requirements. The LV and RV cavities are formed between an LV free wall segment and a septal wall segment and between the septal wall segment and an RV free wall segment, respectively. The area of each wall segment depends on myofiber length in that wall. Pressures are generated by wall tension in the curved wall segments. Equilibria of mechanical forces are used to restrict degrees of freedom for geometry.

The model was tested by manipulating timing of mechanical activation of the various wall segments. Consequences of left bundle branch block (LBBB) have been simulated for septal motion and timing of LV and RV pressure development. Model results were compared with experimental results reported earlier [2, 13-17].

## 2. Methods

### 2.1. Model design

In the model, LV and RV cavities are enclosed by an LV ( $L$ ) and an RV ( $R$ ) free wall segment, respectively. The cavities are separated by a shared septal wall segment ( $S$ ) (Fig. 1). The wall segments are modeled as thick-walled spherical segments. The segments are assumed to be mechanically coupled at midwall. Midwall surface is defined to divide the wall in two spherical shells of equal wall volume. Midwall geometry of a wall segment depends on two variables, i.e., the bulge height of the spherical segment ( $x_s$ ), and the radius of the midwall boundary circle ( $y$ ) (Fig. 1). Midwall curvature, area, and volume of a wall segment can be expressed as a function of these two variables. Since all three wall segments share the same circle of intersection, four variables are needed to describe complete ventricular geometry, i.e.,  $x_R$ ,  $x_S$ ,  $x_L$ , and  $y$ .

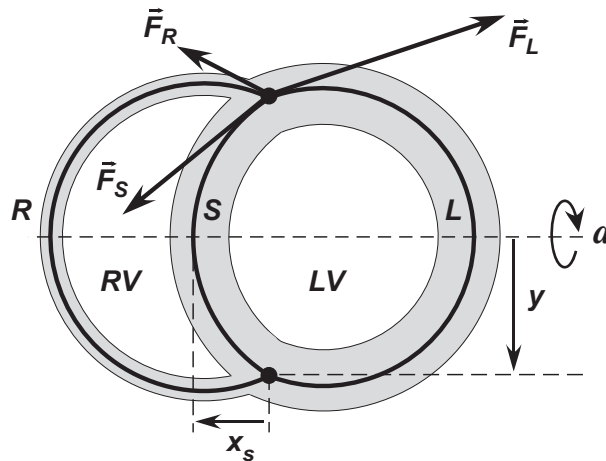


Figure 1: A cross-section of the model of ventricular mechanics. Three thick-walled spherical segments (shaded), i.e., the LV free wall segment ( $L$ ), the RV free wall segment ( $R$ ), and the septal wall segment ( $S$ ) are coupled mechanically. The resulting ventricular composition is rotationally symmetric around axis  $a$  and has a midwall intersection circle crossing this image plane perpendicularly through the thick points. Midwall geometry of the septal wall segment is expressed by bulge height ( $x_s$ ) and the radius ( $y$ ) of the midwall intersection circle. In this intersection each wall segment exerts a force ( $F$ ) caused by wall tension.

The core of the CircAdapt model is a set of first-order differential equations describing state-variables such as ventricular cavity volumes and flows through cardiac valves as a function of time [12]. The CircAdapt model requires that RV and LV cavity pressures are expressed as function of the related cavity volumes. Since in the new model ventricular geometry is defined by four parameters, and only two volumes are known as input values, two remaining geometric parameters have to be solved. This is done by stating equilibrium of forces in the intersection of the wall segments. In Fig. 2, the sequence of calculations within the ventricular module is shown graphically.

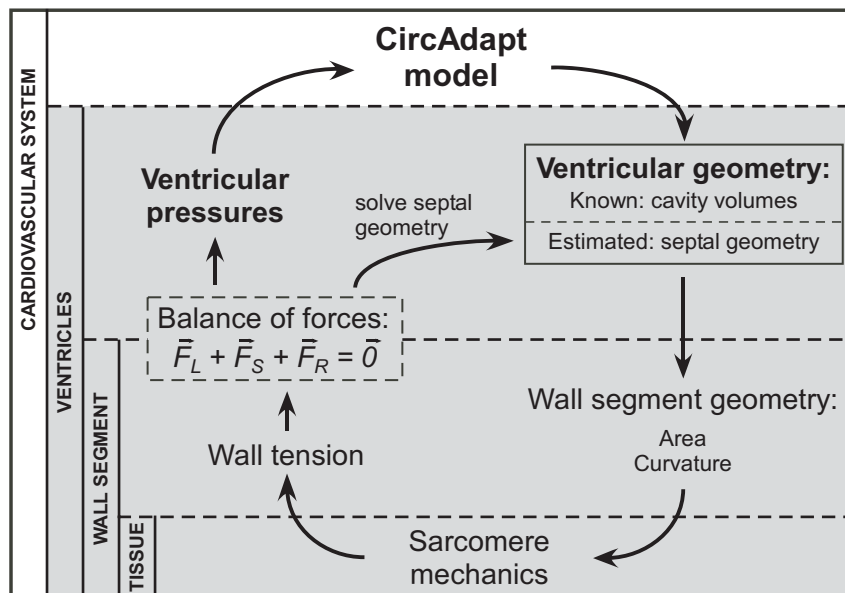


Figure 2: Flowchart of the new ventricular module (shaded area), describing ventricular mechanics up to and including the level of the myocardial tissue, as implemented within the framework of the CircAdapt model of the cardiovascular system [12]. Ventricular pressures are calculated as a function of cavity volumes. Degrees of freedom in septal geometry are solved by achieving balance of forces. Then, ventricular cavity and wall mechanics as well as sarcomere mechanics are known.

Starting with LV and RV volumes and an estimate of septal bulge height  $x_s$  and radius  $y$  of the intersection circle, for all three segments, bulge height and segment radius are calculated. Next, for each segment, midwall area and curvature is calculated. From midwall area and curvature, sarcomere extension is calculated. Myofiber stress is calculated with constitutive equations of the sarcomere incorporating Hill's sarcomere force-velocity relation and Starling's sarcomere length-contractility relation, as previously described in detail by Arts

*et al.* [12]. Using segment geometry, total radial and axial force components of midwall tension acting on the intersection circle are calculated. Thus, force balance provides two equations, which are solved numerically by proper variation of  $x_S$  and  $y$ . Finally, a solution for ventricular geometry is found and LV and RV pressures are calculated from wall tensions, as needed for the CircAdapt model (Fig. 2).

## 2.2. Simulation methods

The model was tested by simulating canine ventricular hemodynamics and mechanics. The first simulation (Control) was assumed to be representative for baseline conditions with synchronously contracting ventricular wall segments. In a simulation of left bundle branch block (LBBB) we imposed asynchronous mechanical activation of the three wall segments, similar to that as observed in dogs with LBBB [18].

Table 1 shows major input parameters used for the Control simulation, representing normal cardiac loading conditions of a dog [16, 19]. The thickness and midwall area of each wall segment were adapted to the loading conditions by using adaptation rules [12]. The LBBB simulation represents an acute experiment in which no structural adaptation has occurred. Thus, with LBBB, size and weight of the wall segments were the same as in Control. Mechanical activation of the septum and LV free wall were delayed by 30 ms and 70 ms relative to the RV free wall, respectively. These average delay times were derived from animal experiments on mongrel dogs in which acute LBBB was induced by ablating the left branch of the His bundle using a radiofrequency catheter [16, 19].

Table 1. Input parameter values used for the simulations.

Parameter	Value	Unit
Mean arterial blood pressure	10.8	kPa
Cardiac output	60	ml/s
Cardiac cycle time	760	ms
Blood pressure drop over pulmonary circulation	1.33	kPa

The set of differential equations has been solved numerically using the ODE113 function in Matlab 7.1.0 (MathWorks, Natick, MA) with a temporal resolution of 2 ms. Simulation results were compared with experimental results of LV and RV pressure curves and the time course of septal motion.

### 3. Results

Simulation results of LV and RV hemodynamics for control and LBBB are shown in Fig. 3. In the Control simulation, the time courses of pressures, volumes and flows are within the normal physiological range. In case of LBBB, the following hemodynamic changes, indicated by numbers in Fig. 3, were noted:

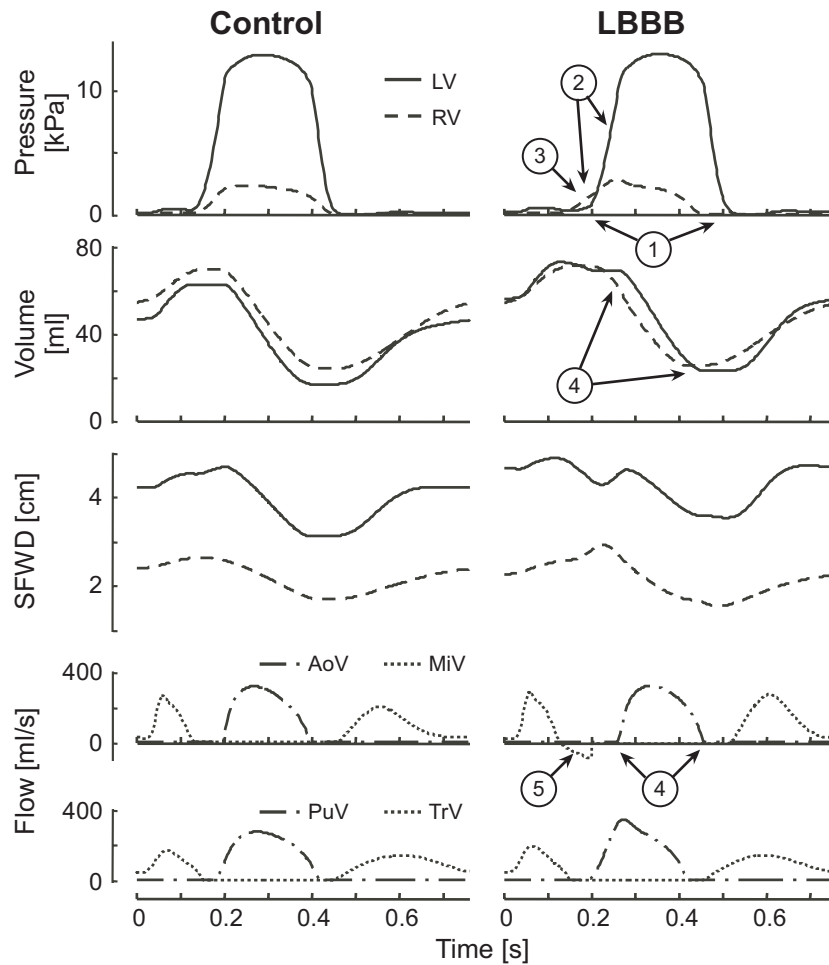


Figure 3: Time courses of left (LV) and right (RV) ventricular hemodynamics as simulated with the CircAdapt model in Control (left panel) and with LBBB (right panel). From top to bottom: LV and RV pressures, LV and RV volumes, septum-to-free wall distance (SFWD) for the LV and RV, flows through aortic (AoV) and mitral valves (MiV), and flows through pulmonary (PuV) and tricuspid valves (TrV). Encircled numbers correspond to changes listed in the text.

1. LV pressure rise and decay were delayed with respect to that of RV pressure.
2. Amplitude of the maximum positive time derivative of LV and RV pressures were both decreased.
3. At the beginning of systole RV pressure exceeds LV pressure.
4. Beginning and end of LV ejection occur later than the corresponding RV events.
5. Mitral flow reverses after atrial contraction.

In Fig. 3, septal-to-free wall distances (SFWD) for both ventricles show also characteristic differences between Control and LBBB. In Control, time courses of RV and LV SFWD follow those of RV and LV volumes quite closely. With LBBB, the septum moves leftward during rise of RV pressure, and rightward shortly thereafter. During the rest of the cardiac cycle septal motion is similar in Control and LBBB.

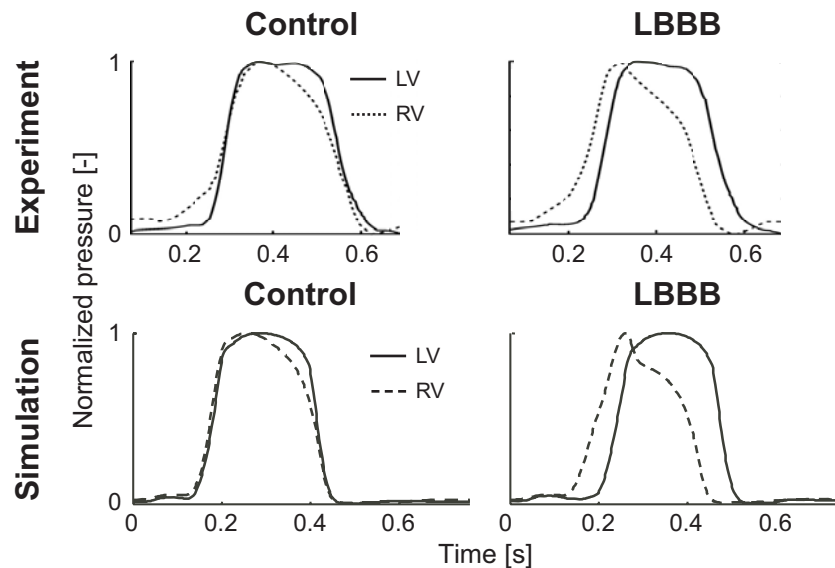


Figure 4: Left ventricular (LV) and right ventricular (RV) pressures normalized to their maxima. Top panels: representative experimental results of LV and RV pressures acquired before (Control) and after (LBBB) ablation of the left branch of the His-bundle in dogs. Adapted from Verbeek *et al.* (2002) [16]. Bottom panels: normalized pressures obtained from the simulations shown in Fig. 3.

Figure 4 shows LV and RV pressure curves normalized to their maximum value. The top panels show these normalized pressures, as obtained experimentally in a dog before and after induction of LBBB [16]. The bottom panels show the corresponding simulated curves. Experiment and simulation are in close agreement on the points already mentioned in relation to Fig. 3.

Moreover, in Fig. 4, experiment and simulation appear in agreement on the increase of asymmetry of the RV pressure curve with LBBB.

Figure 5 shows LV SFWD as derived from typical M-Mode echocardiograms acquired in a dog before (Control) and after induction of LBBB [14]. During LBBB, the experimental LV SFWD curve shows the same typical motion pattern of the septum early in systole as seen in the LBBB simulation.

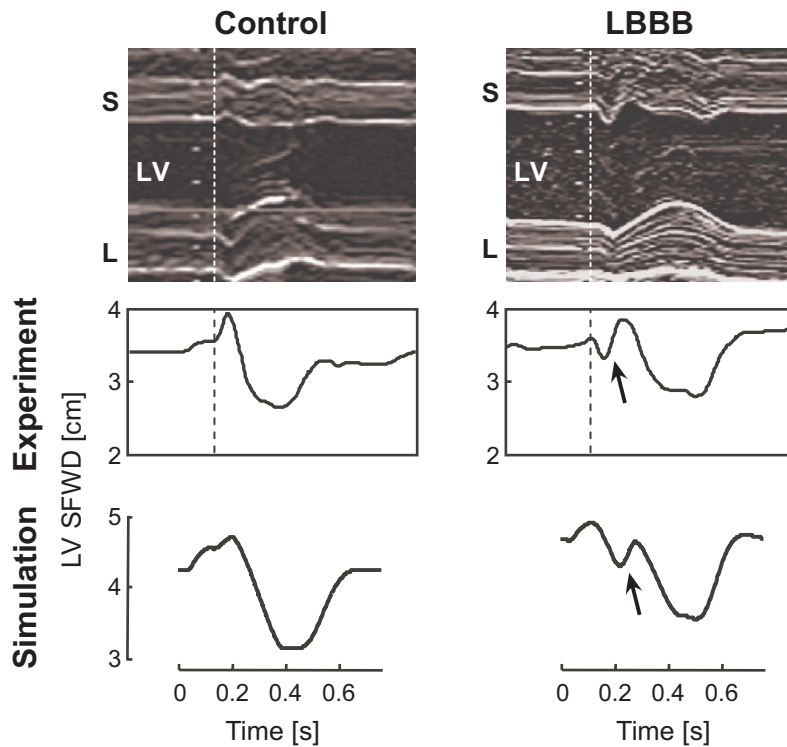


Figure 5: Left ventricular septal-to-free wall distance (LV SFWD) as derived from M-Mode echocardiograms of the left ventricle (LV) in the dog. Adapted from Liu *et al.* (2002) [14]. The septal wall and LV free wall are indicated by S and L, respectively. The left panel was acquired with synchronously contracting ventricles (Control) and the right image after induction of left bundle branch block (LBBB). Start of the QRS complex is indicated by vertical dashed lines. The arrows indicate the early systolic leftward motion of the septum, followed by the paradoxical rightward motion. The simulated curves of LV SFWD, as shown in the bottom panels, appear similar.

Figure 6 shows simulated LV and RV pressure-volume loops and myofiber stress-strain loops of all three wall segments. Stroke volumes do not change because cardiac output and heart rate were fixed in both simulations. In the LBBB simulation, the LV pressure-volume loop is shifted rightward, indicating

ventricular dilatation that is generally considered representative for loss of cardiac contractile function. The areas of the stress-strain loops indicate contractile work of the myofibers per unit of tissue volume in the different wall segments. In Control circumstances, myocardial stroke work per unit of tissue volume is similar in all three segments, i.e., 5.5, 4.7, and 4.6 kPa for LV free wall, septal wall, and RV free wall, respectively. With LBBB, the early activated RV free wall generates clearly less work per unit of tissue volume (4.2 kPa) than the late activated LV free wall (7.8 kPa). Although the septum is later activated than the RV free wall, the septal tissue generates far less work (0.9 kPa).

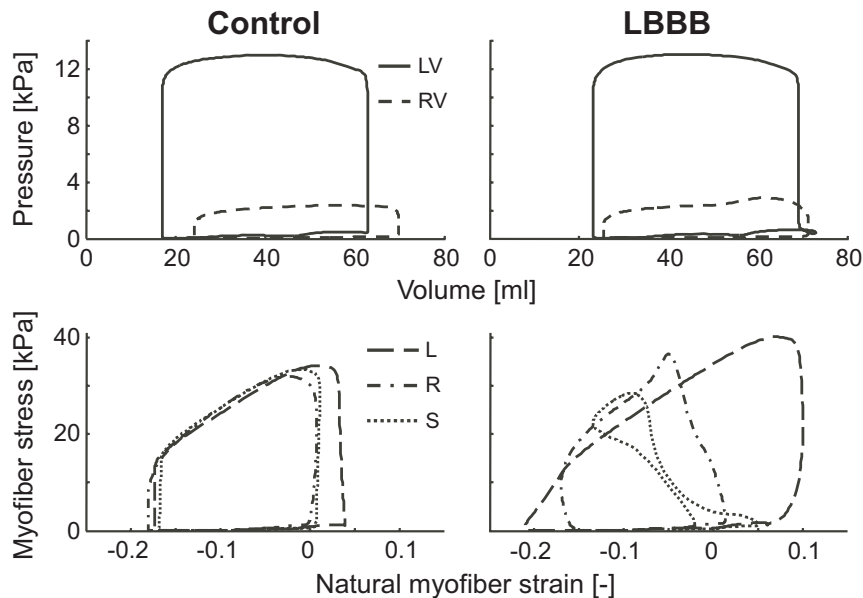


Figure 6: Simulated pressure-volume loops of the left ventricular (LV) and right ventricular (RV) cavities (top panels) and myofiber stress-strain loops of the left ventricular free wall (L), septal wall (S), and the right ventricular free wall (R) (bottom panels). The left panels show results of the Control simulation and the right panels that of the LBBB simulation.

#### 4. Discussion

A lumped module was designed, describing ventricular mechanics with direct ventricular interaction. The ventricular cavities were considered to be formed between three wall segments, being the LV free wall, septum and RV free wall. Mechanical interaction between the walls caused mutual dependency of LV and RV pump function. The three-segment ventricular module was incorporated in the closed-loop CircAdapt model of the complete circulation. Size and weight of

the constituting wall segments were determined by adaptation of the myocardial tissue to imposed mechanical load. A comparison with experimental data [14, 16, 17] demonstrated that simulation results of ventricular mechanics and hemodynamics at baseline and LBBB conditions were surprisingly realistic.

In the model, the atrioventricular valves could close only when the following two conditions were satisfied: 1) ventricular pressure exceeded atrial pressure and 2) the distal ventricular wall segments were mechanically activated. The latter condition mimicked papillary muscle function preventing valvular prolapse when ventricular pressure exceeded pressure in the proximal atrium. In the LBBB simulation, mitral backflow occurred because LV pressure rose above left atrial pressure before mechanical activation of the LV free wall. As soon as the LV free wall was activated, the mitral valve closed. Patient studies have shown that LBBB patients often have mitral regurgitation possibly as a result of late activation of papillary muscles [20].

Figure 6 showed remarkable changes in the amount of myofiber work done by early and late activated wall segments of the LV. The same qualitative changes in LV regional myofiber work density have been observed in animal experiments in which regional LV pump work was derived from strain analysis of short-axis MR tagging images and simultaneous invasive pressure measurements [17]. In chronic LBBB, these regional differences in work density may be responsible for asymmetric remodeling of the LV wall [19].

A crucial step in the calculation procedure was the estimation of sarcomere extension. The one-fiber model by Arts *et al.* [21], related sarcomere extension to the ratio of cavity volume to wall volume. This model has previously been shown to be applicable to an anisotropic thick-walled structure like a myocardial wall when assuming rotational symmetry and homogeneity of mechanical load in the wall. In our new model, the relation between midwall area and sarcomere extension was derived by applying the one-fiber model to a closed spherical cavity. The resulting relation was then extended to a partial segment of the sphere by considering a fraction of the wall, having the same curvature, wall tension, and transmural pressure difference. The one-fiber model has been shown to be rather insensitive to wall geometry [21]. We expected the present relation between midwall area, curvature, and transmural pressure also to be quite insensitive to actual geometry. However, this fact has not been proven.

The simulation results demonstrated that ventricular interaction through the septum is one very important mechanism for the hemodynamic changes associated with abnormal mechanical activation of the ventricular wall segments. However, another important potential mechanism might be changes in contractility due to asynchronous contraction within each wall segment. Due to its lumped character, this model did not allow description of regional

interactions within each wall segment but was limited to the description of its average sarcomere mechanics.

Experimental data show a decrease of cardiac output by approximately 30% after induction of LBBB [16, 19]. In our simulations, however, cardiac output was the same in the Control and LBBB simulations. In the model, cardiac output affects the forces in the intersection of the three wall segments proportionally, provided LV and RV stroke volumes are the same. Thus, a change of cardiac output as observed in the experiments will only affect the amplitude of septal wall motion (Fig. 5) but not its characteristic course in time.

The mechanical coupling of the three spherical wall segments resulted in a circle of intersection with two degrees of freedom, namely, radial and axial displacement. This ventricular composition resulted in simple equations relating wall segment geometry to sarcomere behavior. Implementation of this ventricular module in the CircAdapt model resulted in a closed-loop system model that related fiber mechanics within the cardiac and vascular walls to hemodynamics realistically. Calculation time was limited to 6 seconds per cardiac cycle on a regular personal computer. Furthermore, the model behaved symmetrically around zero septal curvature, so that inversion of transeptal pressure and septal bulging could be handled. In conclusion, the resulting ventricular module satisfied all requirements mentioned in the introduction.

## **5. Conclusion**

In the lumped CircAdapt model of the complete circulation, a new module was incorporated, representing the heart with realistic left to right ventricular interaction. The ventricular part of the heart was designed as a composition of the LV free wall, the septum, and the RV free wall, encapsulating the LV and RV cavities. In a test simulation, ventricular hemodynamics and septal motion during normal synchronous activation was compared with these variables during left bundle branch block. Simulated time courses of ventricular pressures and septal motion were in close agreement with experimental findings. The newly developed three-segment module, describing ventricular mechanics with direct ventricular interaction, is a promising tool in realistic simulation of right heart function and septal motion under normal as well as pathologic circumstances, using the framework of the CircAdapt model.

## **Acknowledgments**

This research was financially supported by Actelion Pharmaceuticals Nederland B.V. (Woerden, The Netherlands).

## References

1. I. Kingma, J. V. Tyberg, and E. R. Smith, *Circulation* **68**, 1304 (1983).
2. W. C. Little, R. C. Reeves, J. Arciniegas, R. E. Katholi, and E. W. Rogers, *Circulation* **65**, 1486 (1982).
3. A. E. Baker, R. Dani, E. R. Smith, J. V. Tyberg, and I. Belenkie, *Am J Physiol* **275**, H476 (1998).
4. C. O. Olsen, G. S. Tyson, G. W. Maier, J. A. Spratt, J. W. Davis, and J. S. Rankin, *Circ Res* **52**, 85 (1983).
5. B. K. Slinker and S. A. Glantz, *Am J Physiol* **251**, H1062 (1986).
6. R. Beyar, S. J. Dong, E. R. Smith, I. Belenkie, and J. V. Tyberg, *Am J Physiol* **265**, H2044 (1993).
7. D. C. Chung, S. C. Niranjani, J. W. Clark, Jr., A. Bidani, W. E. Johnston, J. B. Zwischenberger, and D. L. Traber, *Am J Physiol* **272**, H2942 (1997).
8. J. B. Olansen, J. W. Clark, D. Khoury, F. Ghorbel, and A. Bidani, *Comput Biomed Res* **33**, 260 (2000).
9. W. P. Santamore and D. Burkhoff, *Am J Physiol* **260**, H146 (1991).
10. B. W. Smith, J. G. Chase, G. M. Shaw, and R. I. Nokes, *Physiol Meas* **27**, 165 (2006).
11. Y. Sun, M. Beshara, R. J. Lucariello, and S. A. Chiaramida, *Am J Physiol* **272**, H1499 (1997).
12. T. Arts, T. Delhaas, P. Bovendeerd, X. Verbeek, and F. W. Prinzen, *Am J Physiol Heart Circ Physiol* **288**, H1943 (2005).
13. A. S. Abbasi, L. M. Eber, R. N. MacAlpin, and A. A. Kattus, *Circulation* **49**, 423 (1974).
14. L. Liu, B. Tockman, S. Girouard, J. Pastore, G. Walcott, B. KenKnight, and J. Spinelli, *Am J Physiol Heart Circ Physiol* **282**, H2238 (2002).
15. I. G. McDonald, *Circulation* **48**, 272 (1973).
16. X. A. Verbeek, K. Vernoooy, M. Peschar, T. Van Der Nagel, A. Van Hunnik, and F. W. Prinzen, *Am J Physiol Heart Circ Physiol* **283**, H1370 (2002).
17. F. W. Prinzen, W. C. Hunter, B. T. Wyman, and E. R. McVeigh, *J Am Coll Cardiol* **33**, 1735 (1999).
18. X. A. Verbeek, A. Auricchio, Y. Yu, J. Ding, T. Pochet, K. Vernoooy, A. Kramer, J. Spinelli, and F. W. Prinzen, *Am J Physiol Heart Circ Physiol* **290**, H968 (2006).
19. K. Vernoooy, X. A. Verbeek, M. Peschar, H. J. Crijns, T. Arts, R. N. Cornelussen, and F. W. Prinzen, *Eur Heart J* **26**, 91 (2005).
20. A. Soyama, T. Kono, T. Mishima, H. Morita, T. Ito, M. Suwa, and Y. Kitaura, *J Card Fail* **11**, 631 (2005).
21. T. Arts, P. H. Bovendeerd, F. W. Prinzen, and R. S. Reneman, *Biophys J* **59**, 93 (1991).